High Transmembrane Voltage Raised by Close Contact Initiates Fusion Pore

Bing Bu[1†], Zhiqi Tian[2†], Dechang Li[1*] and Baohua Ji[1*]

[1] Biomechanics and Biomaterials Laboratory, Department of Applied Mechanics, Beijing Institute of Technology, Beijing, China, [2] Key Laboratory of Biomedical Information Engineering of Ministry of Education, Center for Mitochondrial Biology and Medicine, School of Life Science and Technology, Xi'an Jiaotong University, Xi'an, China

Membrane fusion lies at the heart of neuronal communication but the detailed mechanism of a critical step, fusion pore initiation, remains poorly understood. Here, through atomistic molecular dynamics simulations, a transient pore formation induced by a close contact of two apposed bilayers is firstly reported. Such a close contact gives rise to a high local transmembrane voltage that induces the transient pore formation. Through simulations on two apposed bilayers fixed at a series of given distances, the process in which two bilayers approaching to each other under the pulling force from fusion proteins for membrane fusion was mimicked. Of note, this close contact induced fusion pore formation is contrasted with previous reported electroporation under *ad hoc* applied external electric field or ionic charge in-balance. We show that the transmembrane voltage increases with the decrease of the distance between the bilayers. Below a critical distance, depending on the lipid composition, the local transmembrane voltage can be sufficiently high to induce the transient pores. The size of these pores is approximately 1∼2 nm in diameter, which is large enough to allow passing of neurotransmitters. A resealing of the membrane pores resulting from the neutralization of the transmembrane voltage by ions through the pores was then observed. We also found that the membrane tension can either prolong the lifetime of transient pores or cause them to dilate for full collapse. This result provides a possible mechanism for fusion pore formation and regulation of pathway of fusion process.

Keywords: membrane fusion, transmembrane voltage, fusion pore formation, exocytosis, mechanical force

INTRODUCTION

Membrane fusion, as an important and ubiquitous cellular process, lies at the heart of neuronal communication wherein neurotransmitters are quickly released from synaptic vesicles following fusion with the presynaptic membrane. During this process, an initial fusion pore is assumed to be created between the two apposed membranes, and this tiny pore may either expand to a larger one or close back, which leads to two kinds of fusion mode (Alabi and Tsien, 2013). One type of fusion mode called full fusion (FF) requires fusion pore expand to the point where the vesicle membrane flattens into the plasma membrane surface, leading to complete luminal content release(Chernomordik and Kozlov, 2003; Jackson and Chapman, 2008); the other type of fusion mode proceeds without pore expansion, where vesicles transiently fuse at the plasma membrane to release a part of their neurotransmitters (Richards, 2009) without full collapse into the plasma

membrane known as "kiss-and-run" fusion (KR) (He and Wu, 2007; Zhang et al., 2009). Although, the experimental results on membrane fusion at synapses are mounting (He and Wu, 2007), it is difficult to directly image the fusion process at sufficient resolution, thus the molecular mechanism of the fusion initiation is still unclear.

In addition, it is also unclear how the fusion process is regulated *in vivo*. For instance, there is a long standing debate over FF and KR fusion for the regulating mechanisms behind the synaptic release (Marx, 2014). One of the important issues in the debate is an incomplete understanding of the structural mechanics of the membrane under the force of fusogenic proteins (Jahn et al., 2003; Rizo and Rosenmund, 2008), and how these forces act on the membrane during the fusion process. It is known that when a small membrane pore is created (Chernomordik and Kozlov, 2008), it might either close or expand (Chanturiya et al., 1997; Wong et al., 2007; Diao et al., 2012). The reversible fusion pore modality, corresponding to KR fusion, enables a rapid and economical vesicle recycling compared to FF that may require ancillary proteins to retrieve fused vesicles (He and Wu, 2007). However, how the fusion pore is regulated for the fast synaptic transmission and the exact molecular picture of the pore evolution remains obscure.

Transient pore formation has been observed in many *in vivo* and *in vitro* systems, such as liposomes from yeast vacuoles (Starai et al., 2007; Zucchi and Zick, 2011), mating yeast pairs (Aguilar et al., 2007), cell pairs mediated by influenza fusase hemagglutinin (HA) (Blumenthal and Morris, 1999; Frolov et al., 2003), and proteoliposomes reconstituted with neuronal SNAREs (SNAP [Soluble NSF attachment protein] Receptors) (Dennison et al., 2006; Lai et al., 2013; Gong et al., 2015). And there are also many proposed mechanisms for the opening of the membrane pores through *in silico* simulations, such as transmembrane ionic charge imbalance, external electric and mechanical forces (Müller et al., 2003; Gurtovenko et al., 2010). However, the questions of how transient pores are produced in physiological conditions, and how they are regulated remain enigmatic. Here, through full atom molecular dynamics (MD) simulations, we discovered a fast and transient membrane pore formation when the distance of two apposed bilayers was set below a threshold value. The average size of these pores was of 1~2 nm in diameter, which is large enough for passing neurotransmitters. The initial pore could either shrink or expand depending on the magnitude of membrane tension. The high local transmembrane voltage caused by the close contact of apposed membranes was responsible for the formation of these fast and transient membrane pores. This study might thus shed promising light on the molecular mechanisms of pore formation and evolution.

METHODS

MD Simulation

To simulate the pore formation at the contact of a vesicle with the synaptic membrane, we created two apposed lipid bilayers set at various distances (see **Figure 1**). The lipid bilayers were generated by Membrane Builder online service (Jo et al., 2008, 2009). The simulation system was set up following a similar procedure in our previous studies (Li et al., 2010, 2011, 2015; Lai et al., 2015; Xu et al., 2015). The system was solvated in a ~23 × 23 × 20 nm³ TIP3P (Jorgensen et al., 1983) water box, with ~210,000 water molecules and potassium ions added to neutralize the system. All the simulations were performed using GROMACS package (Van Der Spoel et al., 2005) with CHARMM36 force field (Klauda et al., 2010). Periodic boundary condition was applied and the temperature was coupled to 300 K with V-rescale algorithm (Bussi et al., 2007). The pressure was coupled to 1 bar with Parrinello-Rahman approach (Parrinello and Rahman, 1981). The LINCS algorithm (Hess, 2008) was applied to constrain the covalent bonds with H-atoms. The time step of the simulations is 2.0 fs. The cut-off of the non-bonded interactions was set to 10 Å. The particle mesh Ewald (PME) (Essmann et al., 1995) method was used to calculate the long-range electrostatic interactions. The non-bonded pairs were updated in every 10 steps. Each MD simulation was performed independently for three replicates. The simulation system was validated by its reproducing the stalk-like structure in experiments under dehydration condition (Yang and Huang, 2002). All graphics and visualization analysis were processed using the VMD program (Humphrey et al., 1996).

Here the lipid composition was adopted as Chol:DOPC:POPE:POPS with different ratio of percentage as (20:45:20: 15%), (20:48:20:12%), (20:51:20:9%), (20:54:20:6%), and (20: 55.5:20:4.5%). Chol, DOPC, POPE, POPS are abbreviation of cholesterol, 1,2-dioleoyl-sn-glycero-3-phosphocholine, 1-palmitoyl-2-oleoyl-sn-glycero-3-phosphoethanolamine, and 1-palmitoyl-2-oleoyl-sn-glycero-3-phenylserine, respectively.

In the molecular dynamics simulations, we carried out simulations on two bilayers set at various membrane distances, where the distance D was chosen by reducing its value from 6 nm, in 0.5 nm steps (see Figure S1), for mimicking the approaching process of two apposed bilayer under the pulling force of fusion protein for membrane fusion. Each simulation was done at a given constant membrane distance.

The ions were uniformly distributed in the three cytosol/fluid regions, i.e., the vesicle cytosol, cellular cytosol between the vesicle and presynaptic membranes, and the interstitial fluid around the synapse, as shown in Figure S1. The ionic concentration (potassium) was about 0.04~0.15 mol/L, depending on the lipid composition and their percentage. The density of water was 1 g/cm³. Note that for specific lipid composition, the density of water and ions was kept constant. In the simulation, we chose potassium ions as the only ions in the system without chloride ions. For double check, we also did simulations with both potassium and chloride ions. In the presence of chloride ions, we put more potassium ions to neutralize the system. Our results showed that they had similar results as those in the absence of chloride ions.

For simulating the pore evolution under membrane tension, we built membrane tension Γ by applying pressure on the simulation box, given by $\Gamma = L_Z (P_Z - P_{Lat})$, where L_Z is the length of the simulation box in the Z direction, P_Z is the pressure along the Z direction, and P_{Lat} is the pressure along lateral direction in the membrane plane (Leontiadou et al., 2004).
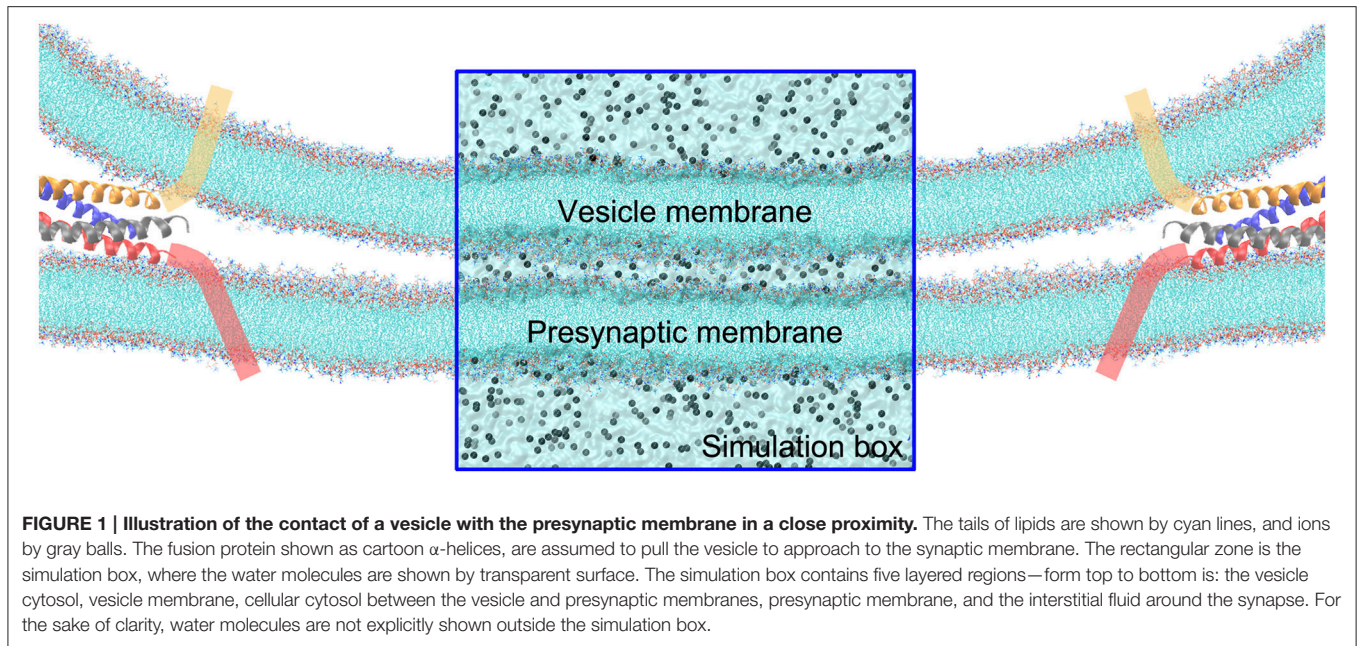
FIGURE 1 | Illustration of the contact of a vesicle with the presynaptic membrane in a close proximity. The tails of lipids are shown by cyan lines, and ions by gray balls. The fusion protein shown as cartoon α-helices, are assumed to pull the vesicle to approach to the synaptic membrane. The rectangular zone is the simulation box, where the water molecules are shown by transparent surface. The simulation box contains five layered regions—form top to bottom is: the vesicle cytosol, vesicle membrane, cellular cytosol between the vesicle and presynaptic membranes, presynaptic membrane, and the interstitial fluid around the synapse. For the sake of clarity, water molecules are not explicitly shown outside the simulation box.

Calculation of the Transmembrane Voltage

To calculate the transmembrane voltage in MD simulations, we adopted the procedure proposed by Tieleman by solving a one dimensional Poisson's equation (Tieleman, 2004). Firstly, the charge density along the Z direction $\rho(Z)$ was calculated by averaging the net charges over the membrane plane. The electric potential can be obtained by solving the one dimensional Poisson's equation, i.e., $\Phi(Z) = -\frac{1}{\varepsilon} \int_0^Z \int_0^{Z'} \rho(Z'') \, dZ'' dZ' + \Phi(0)$, where $\Phi(0)$ was chosen as zero at the axis of symmetry of the system at Z = 0. The difference of the electric potential through the membrane gives the transmembrane voltage.

Theoretical Model of Electric Potential

In our model, we used five layers to consider the five regions at the contact between the vesicle and presynaptic membrane: the cytosol in vesicle, R_1, the vesicle membrane R_{m1}, the cellular cytosol between vesicle and presynaptic membrane, R_2, the presynaptic membrane R_{m2}, and the interstitial fluid around synapse, R_3 (see **Figure 2**). Since we considered the local contact region between vesicle and presynapse, we assumed that the distribution of charges was uniform in each layer. For a neutralized system, the charge density should satisfy

$$\rho_1 H_L + \rho_3 H_L + \rho_2 D + \rho_{m1} H_m + \rho_{m2} H_m = 0 \qquad (1)$$

where ρ_1, ρ_2, ρ_3, ρ_{m1}, and ρ_{m2} are charge density in layers R_1, R_2, R_3, R_{m1}, and R_{m2}, respectively. H_L is the thickness of layers R_1 and R_3 (here we adopted that the thickness of the two domains is identical), H_m is the thickness of membrane, and D is the distance between the two apposed membranes. In this situation, the electric potential satisfies the one dimensional

Poisson-Boltzmann equation,

$$\frac{d^2\Phi(Z)}{dZ^2} = -\frac{\rho(Z)}{\varepsilon} \qquad (2)$$

where $\Phi(Z)$ is the electric potential along the Z direction, $\rho(Z)$ is the charge density and ε the dielectric constant. We set $\varepsilon = 3$ according to experimental measurement by Gramse et al. (2013). And we obtained the electric potential as

$$\Phi(Z) = -\frac{1}{\varepsilon} \int_0^Z \int_0^{Z'} \rho(Z'') \, dZ'' dZ' \qquad (3)$$

The result of the integral in Equation (3) can be found in Supplementary Material. Thus the transmembrane voltage of the vesicle membrane can be calculated as

$$\Delta V_1 = -\frac{1}{\varepsilon}(\frac{1}{2}\rho_{m1} H_m + \rho_{m2} H_m + \rho_2 D + \rho_3 H_L) H_m \qquad (4)$$

and the corresponding voltage of the presynaptic membrane is

$$\Delta V_2 = -\frac{1}{\varepsilon}(\frac{1}{2}\rho_{m2} H_m + \rho_{m1} H_m + \rho_2 D + \rho_1 H_L) H_m \qquad (5)$$

As shown in Equations (4 and 5), because ρ_{m1} and ρ_{m2} are negative, ΔV_1 and ΔV_2 linearly increase with the reduction of the inter-membrane distance D. If we assume $\rho_1 = \rho_3$, and $\rho_{m1} = \rho_{m2} = \rho_m$, we have

$$\Delta V = \Delta V_1 = \Delta V_2 = -\frac{1}{2\varepsilon}(\rho_m H_m + \rho_2 D) H_m \qquad (6)$$

RESULTS

Close Contact Induces Transient Pore Formation

To understand the very early stage of membrane fusion when the vesicle and presynaptic membranes get close, we simulated two apposed membranes fixed at a series of given distances using MD simulations, mimicking the docking process pulled by SNAREs or other accessory proteins, as shown in **Figure 1**. By using a smaller distance between membranes below a critical value (discussed below), we found the formation of tiny pores on the membranes (**Figure 3**). When the two membranes were within ~5 nm, a water line first formed across the thickness of membrane in several nanoseconds, followed by the formation of a transient pore, like a water channel, spanning the membranes (**Figure 3B**). Then the transient pore grew rapidly, causing considerable redistribution of lipid headgroups close to the channel. At the same time, ions can transport through these pore, as shown in **Figure 3B**. The duration of the ion transportation was very short (approximately 10 ns). Once the ion transportation was finished, the pores healed automatically as the results of balancing charge difference (**Figure 3C**). More details of the pore formation, ions leakage and pore healing can be found in Figure S2 and Movie S1 in Supplementary Material. To examine the physiological relevance of our simulations, the membrane distance was further reduced to mimic a higher degree of dehydration, which induced a stalk-like structure for hemifusion. This result is consistent with previous experiments of Yang and Huang (Yang and Huang, 2002) (see Figure S3) and validates our MD simulations.

To study the molecular mechanisms of the pore formation, we calculated the electric potential in our system. Our results showed that the distribution of electric potential is highly dependent on inter-membrane distance. As the distance between the two membranes decreased, the difference of electric potential across the lipid bilayer, i.e., the transmembrane voltage, rose significantly (**Figure 3D**). This transmembrane voltage formed the driving force for the pore formation, consistent with earlier reports that the transmembrane voltage caused by ionic charge imbalance between the two sides of the membrane (Gurtovenko and Vattulainen, 2005), or by external electric field (Tieleman, 2004; Sun et al., 2011), induces fusion pore and ion trafficking. Meanwhile, in previous studies, the transmembrane voltage was ad-hoc applied on the membrane (Tieleman, 2004; Gurtovenko and Vattulainen, 2005; Sun et al., 2011). Here we found that without the above *ad hoc* conditions, reducing the membrane distance alone was sufficient to cause a dramatic increase in transmembrane voltage capable of producing the driving force necessary for the fusion pore formation. Our simulation showed that the transmembrane voltage for pore formation produced by the close contact is in the range of 0.7~1.2 V, consistent with the value of 0.5~1.5 V used in electroporation experiments (Weaver and Chizmadzhev, 1996). The mean size of the pores was round 1–2 nm (see **Figures 3G–I**), which is large enough for the passing of small neurotransmitters (Zhang et al., 2009).
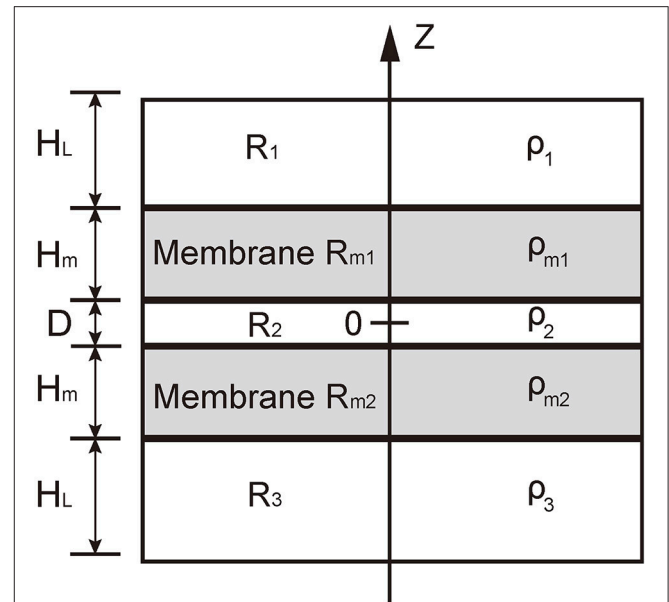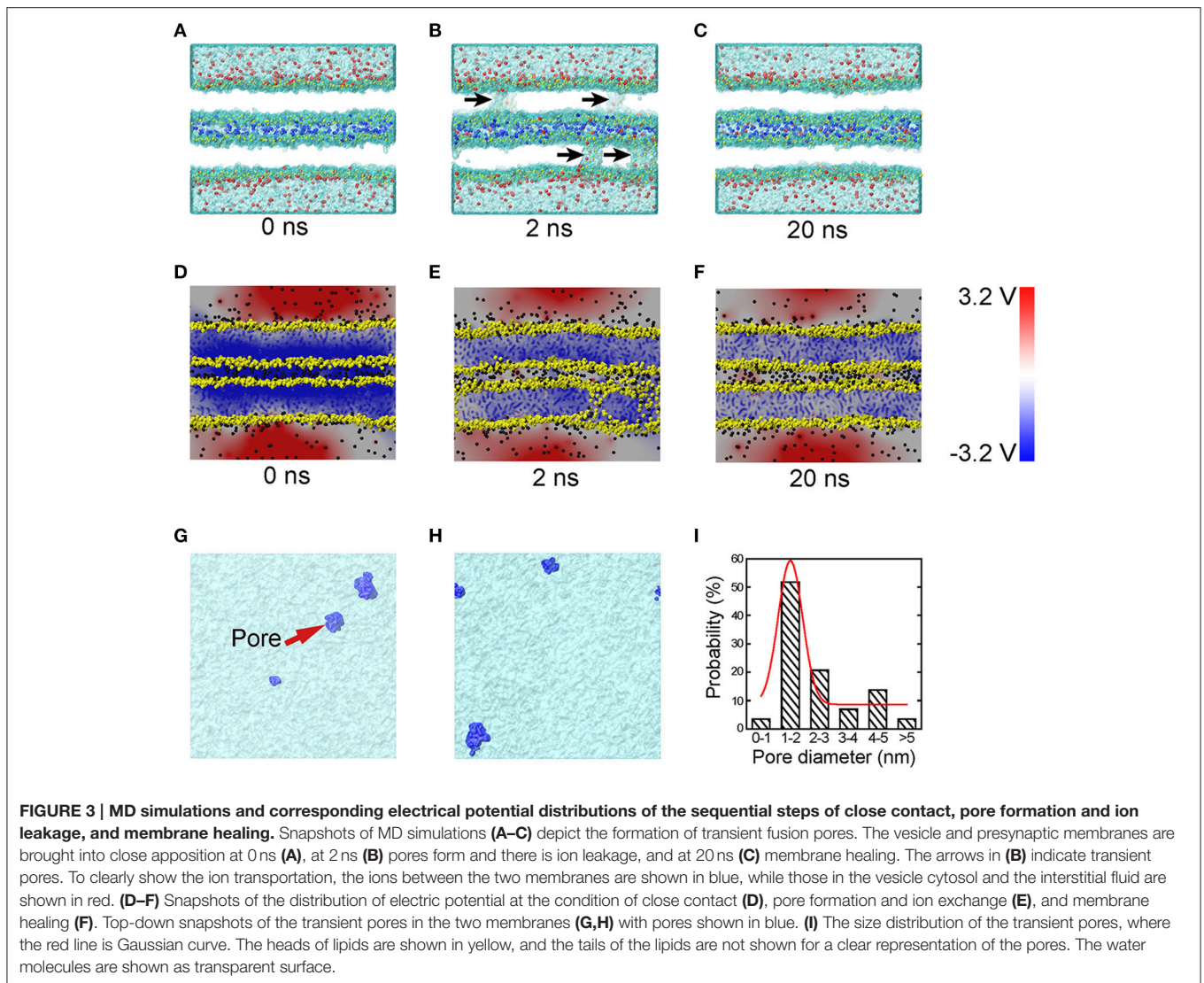

FIGURE 2 | Illustration of the theoretical model. The domain R_1 represents the cytosol in vesicle, R_2 represents the cytosol between the vesicle and the presynaptic membranes, and R_{m1} represents interstitial fluid around synapse. R_{m1} and R_{m2} represents the vesicle membranes and presynaptic membrane, respectively. The charge density in domains R_1 and R_3 are denoted by ρ_1 and ρ_3, respectively; that in domain R_2 by ρ_2, and that in the domains R_{m1} and R_{m2} by ρ_{m1} and ρ_{m2}, respectively.

Transmembrane Voltage vs. the Membrane Distance

To understand the mechanism of transmembrane voltage rising with the decrease of membrane distance, we employed a physical model to derive the field of electric potential in the apposed membranes as a function of the membrane distance (**Figure 2**). For a given ion distribution corresponding our MD simulations, we obtained the analytical solution of the field of electric potential and in particular, a linear relationship between the transmembrane voltage and the membrane distance for a close contact (see Methods). We found that when the membrane distance was less than ~5 nm, the profile of the electric potential in each membrane became severely asymmetric with respect to the central line of the lipid bilayer thus producing a high transmembrane voltage (**Figure 4A**). However, after the ion leakage, the profile of the electric potential almost resumed its symmetry, resulting in a reduced transmembrane voltage (**Figures 3F, 4A**). This prediction is consistent with observations from our MD simulations (Figure S4). Moreover, it clearly indicates that the transmembrane voltage, produced by the close contact of the apposed membranes, was the driving force for the transient pore formation.

Threshold Values of Membrane Distance

To find the threshold value of membrane distance for the pore formation, we performed a series of MD simulations at different membrane distances. We defined the critical distance as the
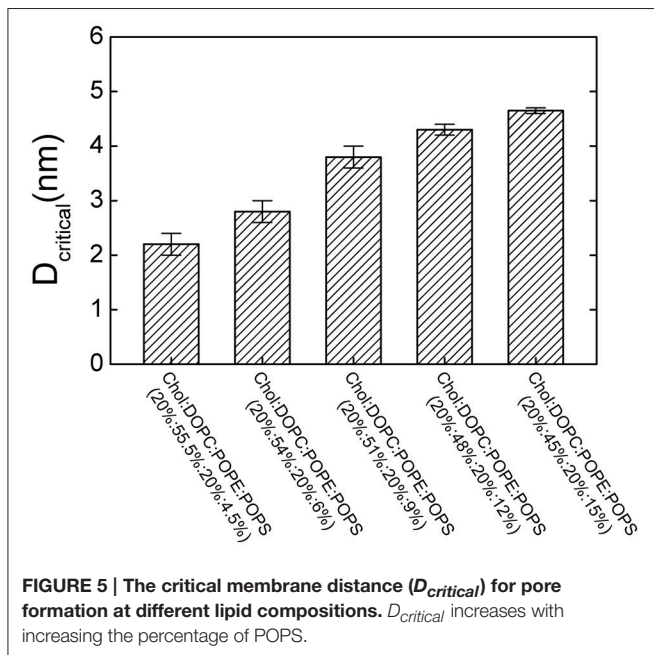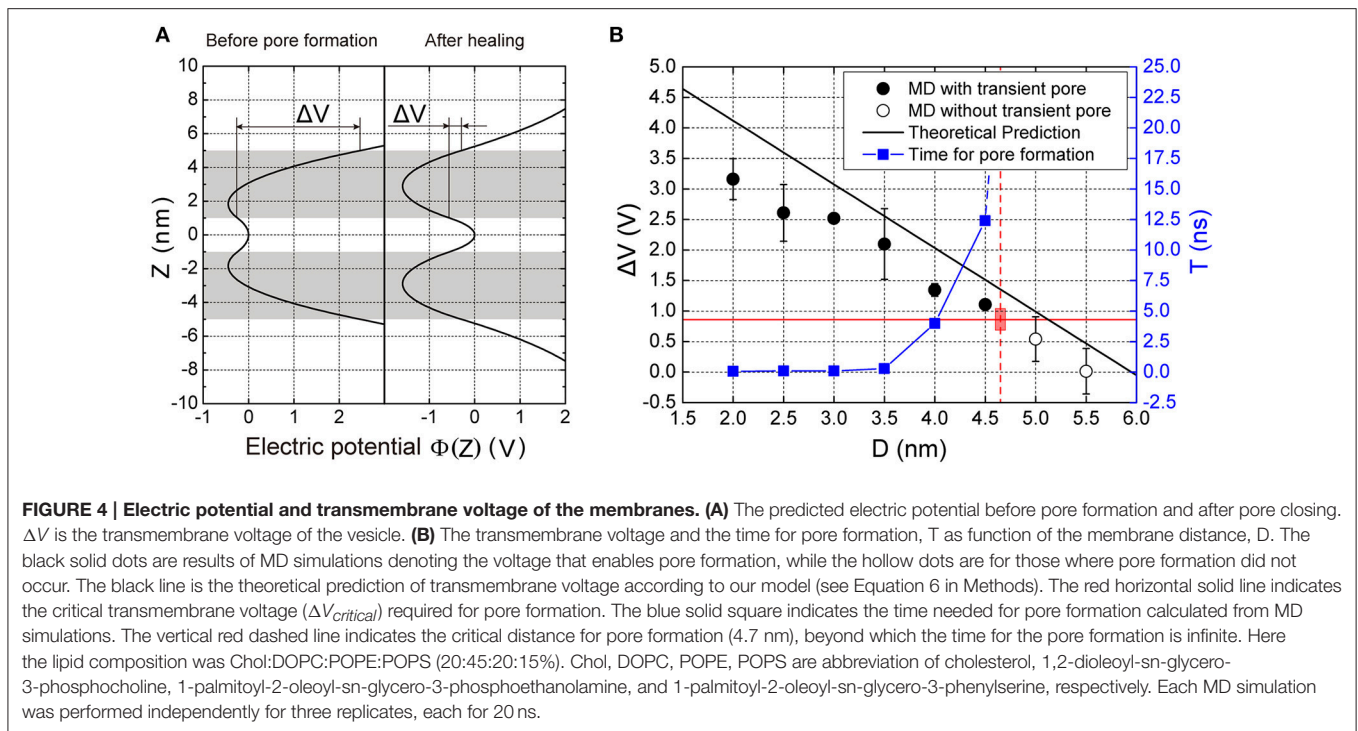
FIGURE 3 | MD simulations and corresponding electrical potential distributions of the sequential steps of close contact, pore formation and ion leakage, and membrane healing. Snapshots of MD simulations **(A–C)** depict the formation of transient fusion pores. The vesicle and presynaptic membranes are brought into close apposition at 0 ns **(A)**, at 2 ns **(B)** pores form and there is ion leakage, and at 20 ns **(C)** membrane healing. The arrows in **(B)** indicate transient pores. To clearly show the ion transportation, the ions between the two membranes are shown in blue, while those in the vesicle cytosol and the interstitial fluid are shown in red. **(D–F)** Snapshots of the distribution of electric potential at the condition of close contact **(D)**, pore formation and ion exchange **(E)**, and membrane healing **(F)**. Top-down snapshots of the transient pores in the two membranes **(G,H)** with pores shown in blue. **(I)** The size distribution of the transient pores, where the red line is Gaussian curve. The heads of lipids are shown in yellow, and the tails of the lipids are not shown for a clear representation of the pores. The water molecules are shown as transparent surface.

distance above which the pore formation will not happen in up to 20 ns in our simulation (**Figure 4B**). When the distance, D, was larger than a critical value (~5 nm), the voltage was nearly zero because of the symmetry of the field of electric potential in the membrane. But as the distance decreased, the voltage increased, being negatively proportional to the distance (see Equation 6 in Methods). Referring to our MD simulations, a series of membrane distance D was chosen by reducing its value from 6 nm, in 0.5 nm steps, for the lipid composition Chol:DOPC:POPE:POPS (20:45:20:15%). In these settings, we found that the transmembrane voltage produced by the close contact could be up to >3 V, consistent with previous results produced by the transmembrane ionic charge imbalance (Gurtovenko and Vattulainen, 2005). We found that when the distance was larger than 5 nm, there was no transient pore formation. But when D became smaller, pore formation could be observed. In addition, the smaller the distance is, the faster the pore could form (**Figure 4B**, blue line). These results

suggest there is a threshold value for the inter-membrane distance required for the transient pore formation.

Effect of Lipid Composition on Fusion Pore Formation Threshold

To investigate the contribution of the lipid composition in fusion pore formation, we modified our simulations to adopt various lipid compositions by changing the percentage of POPS, which modulates the charge density on the membrane. Our results showed that the threshold value of membrane distance for pore formation was highly dependent on the percentage of POPS (**Figure 5**). For example, we found that reducing the percentage of POPS in both membranes generally reduced the threshold value due to dissipated charge density of the membrane. The lower the percentage of the POPS, the smaller the critical distance needed, and thus the more difficult the pore formation. This result also emphasizes why two membranes should be brought close together for fusion: only a membrane

FIGURE 4 | Electric potential and transmembrane voltage of the membranes. (A) The predicted electric potential before pore formation and after pore closing. ΔV is the transmembrane voltage of the vesicle. **(B)** The transmembrane voltage and the time for pore formation, T as function of the membrane distance, D. The black solid dots are results of MD simulations denoting the voltage that enables pore formation, while the hollow dots are for those where pore formation did not occur. The black line is the theoretical prediction of transmembrane voltage according to our model (see Equation 6 in Methods). The red horizontal solid line indicates the critical transmembrane voltage ($\Delta V_{critical}$) required for pore formation. The blue solid square indicates the time needed for pore formation calculated from MD simulations. The vertical red dashed line indicates the critical distance for pore formation (4.7 nm), beyond which the time for the pore formation is infinite. Here the lipid composition was Chol:DOPC:POPE:POPS (20:45:20:15%). Chol, DOPC, POPE, POPS are abbreviation of cholesterol, 1,2-dioleoyl-sn-glycero-3-phosphocholine, 1-palmitoyl-2-oleoyl-sn-glycero-3-phosphoethanolamine, and 1-palmitoyl-2-oleoyl-sn-glycero-3-phenylserine, respectively. Each MD simulation was performed independently for three replicates, each for 20 ns.

FIGURE 5 | The critical membrane distance ($D_{critical}$) for pore formation at different lipid compositions. $D_{critical}$ increases with increasing the percentage of POPS.

distance smaller than the threshold value can produce a sufficiently high transmembrane voltage that can induce pore formation.

Note that we did not consider the asymmetry of lipid composition between the inner and outer leaflet of cell membrane (Svennerholm, 1968; Devaux, 1991). Although, the asymmetry may affect the process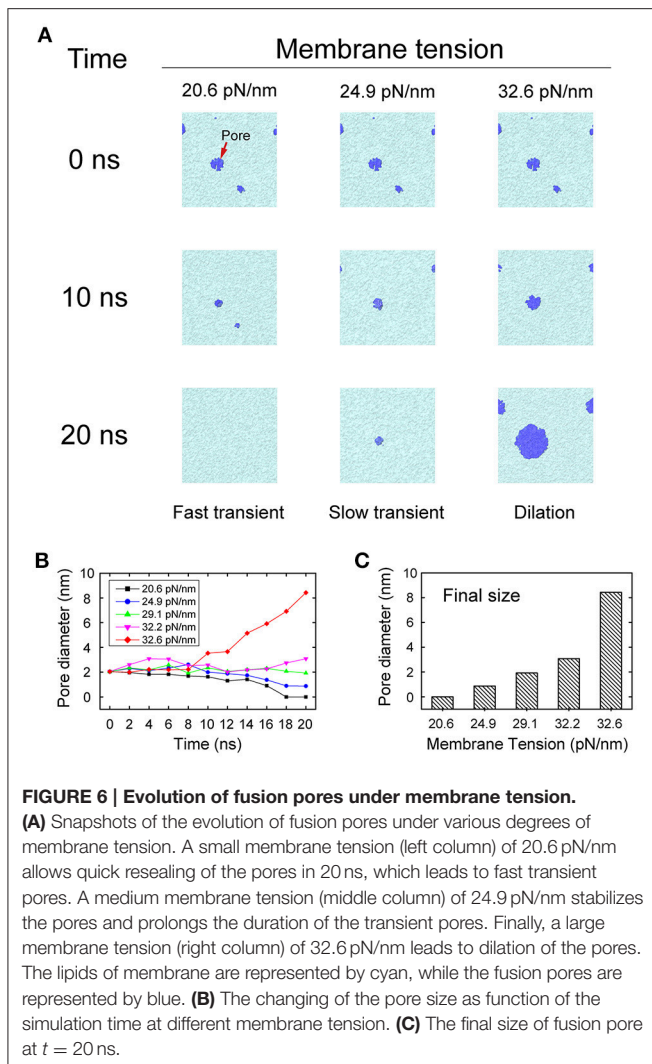 of fusion pore formation, it is a secondary factor in the membrane fusion in comparison with the close contact between the membranes. Heterogeneity of lipid composition may also be an influencing factor in the fusion process. For instance, phosphatidylinositol-4,5-bisphosphate (PIP2), a lipid with -5e negative charges, is an important composition that accumulates at the location of fusion site (McLaughlin and Murray, 2005; Graber et al., 2014). But the localized PIP2 mainly interacts with syntaxin proteins during the course of membrane fusion. And the function of fusion protein syntaxin is to pull the two apposed membranes to be close contact, which we had effectively considered by applying pulling force on the membranes. To test the influence of the asymmetric lipid composition and localized PIP2, we performed an additional simulation with 5% PIP2 in the cytoplasmic leaflet which make the two membranes asymmetric, as shown in Figure S5. It shows that the close contact of the two membranes containing localized PIP2 could still give rise to a high local transmembrane voltage which induced the pore formation.

Force Regulates the Pore Evolution

During membrane fusion, fusion proteins apply not only vertical force to pull the vesicle close to the presynaptic membrane, but also lateral force along the membrane which produces a local membrane tension. To mimic this behavior of fusion proteins, we imposed a lateral force on the membrane once the pores were initiated, to study how the local membrane tension regulates its structural evolution. We found that when the tension was small (20.6 pN/nm), the membrane pore shrank and resealed quickly in less than 20 ns. However, when the tension was increased (24.9 pN/nm), the resealing process of

FIGURE 6 | Evolution of fusion pores under membrane tension.
(A) Snapshots of the evolution of fusion pores under various degrees of
membrane tension. A small membrane tension (left column) of 20.6 pN/nm
allows quick resealing of the pores in 20 ns, which leads to fast transient
pores. A medium membrane tension (middle column) of 24.9 pN/nm stabilizes
the pores and prolongs the duration of the transient pores. Finally, a large
membrane tension (right column) of 32.6 pN/nm leads to dilation of the pores.
The lipids of membrane are represented by cyan, while the fusion pores are
represented by blue. **(B)** The changing of the pore size as function of the
simulation time at different membrane tension. **(C)** The final size of fusion pore
at $t = 20$ ns.

the fusion pore became slower. When the tension was further
increased (32.6 pN/nm) the fusion pore started to expand and the
vesicle began to collapse into the membrane (**Figure 6**). In our
simulations, the first two cases, where the membranes resealed,
are correspond to the scenarios of fast and slow transient pore
for KR fusion, while the third case corresponds to the pore
dilation of FF. This result clearly indicates that the stability and
evolution of the fusion pore, and the selection of fusion pathways
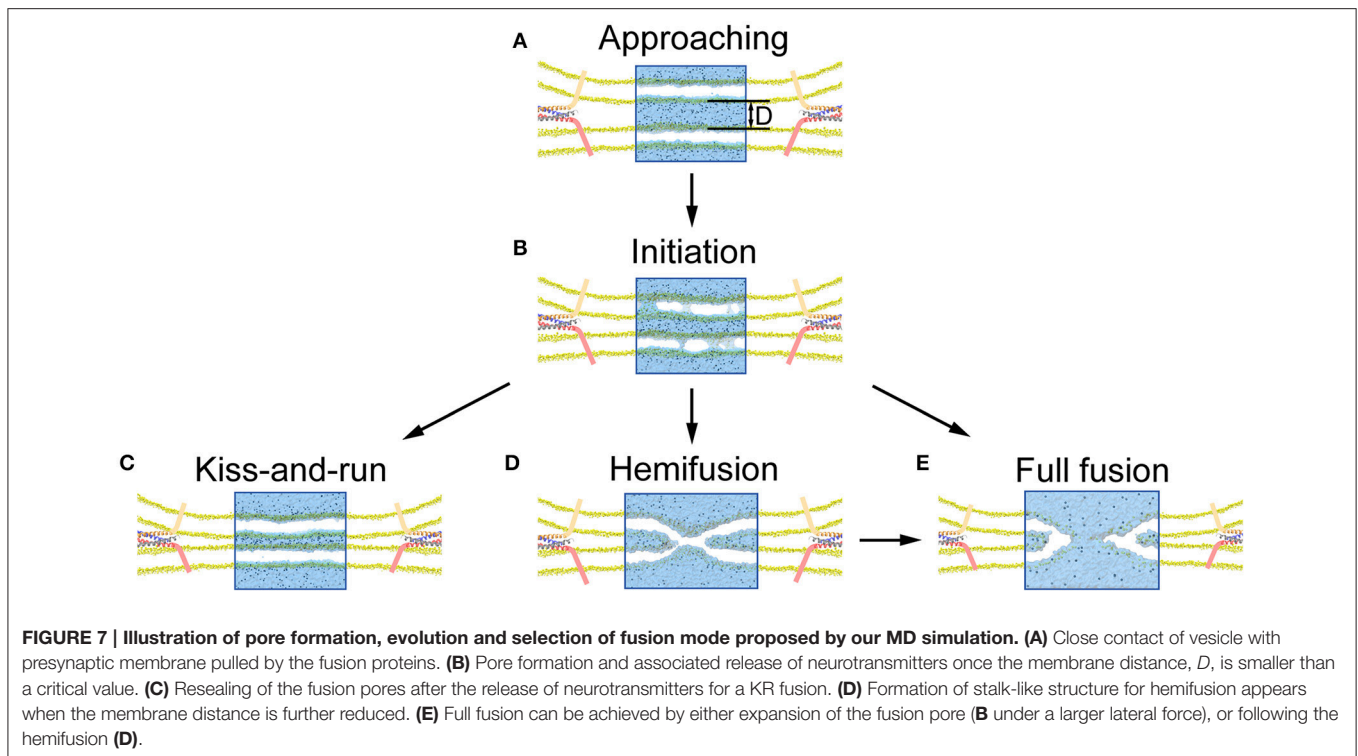between KR fusion and FF, could be regulated by the membrane
tension.

DISCUSSION

This study suggests a feasible mechanism for pore formation
in membrane fusion: a close contact of membranes could
generate a high transmembrane voltage, which in turn produces
the membrane pores. Note that the close-contact induced
voltage observed in our simulation is contrasted with the *ad
hoc* applied voltage in previous electroporation experiments

(Weaver and Chizmadzhev, 1996). The opening of the fusion
pore, initiated from a voltage-dependent perturbation of lipid
organization at the contact of apposed bilayers, begins with a
lateral parting of headgroups on two membranes for allowing
water molecules to enter the hydrophobic regions (Helm et al.,
1992; Fesce et al., 1994). Although, the transmembrane voltage
can be produced by an *ad hoc* ionic charge imbalance across
membranes (Gurtovenko and Vattulainen, 2005) or external
electric field (Tieleman, 2004; Sun et al., 2011), how cells
modulate the ionic charge imbalance or electric fields in
order to produce the required voltage is not known. In this
study, we showed that the transmembrane voltage can be
generated by reducing the distance between two membranes,
an action that could be carried out by fusion proteins, such
as SNAREs or the calcium sensor, synaptotagmin, etc., (Diao
et al., 2009, 2013; Kyoung et al., 2013; Lai et al., 2014).
Our data agrees with a growing body of work suggesting
that pore formation, stability, and evolution can be subject
to regulation by cellular processes rather than a stochastic
thermodynamic process (Wang et al., 2009; Risselada and
Grubmüller, 2012).

In agreement with previous studies, our results further
support the notion that native proteins are capable of modulating
fusion pore dynamics with additional helps from other proteins
producing differential layers of modulation (Alabi and Tsien,
2013; Lai et al., 2015). We found that the fusion pore dynamics
appeared to be finely modulated by the type and magnitude
of mechanical force exerted on membrane. A vertical force
pulls the vesicle close to the plasma membrane, increasing the
local voltage difference resulting in more pore formation. A
further increase of the vertical force produces a closer contact
for to a stalk-like structure for hemifusion (Figure S3), as
observed in previous experiments (Yang and Huang, 2002;
Zhao et al., 2016). In contrast, we found that the membrane
tension at the contact site induced by the lateral force stabilizes
pore formation and increases pore duration, while a larger
force could induce pore expansion (**Figure 6**). These results
suggest that the fusion dynamics could be regulated by the
force of fusion proteins, and by extension, so as the rate of
neurotransmitter diffusion out of the synaptic vesicle (Richards,
2009; Zhang et al., 2009; Alabi and Tsien, 2013). Since KR
fusion and hemifusion are intermediate states between prime
(un-fused) state and FF, the mechanical forces produced by
fusion machinery proteins could select among KR, hemifusion,
and FF (**Figure 7**), to modify the kinetics of neurotransmitter
release which could ultimately provide a mechanism to regulate
synaptic strength and achieve synaptic plasticity (He and Wu,
2007).

In conclusion, we provided a new mechanism for the initiation
of fusion pore and its evolution through MD simulations of
two membranes being set close together. Subsequent fusion
pore initiation occurred within several nanoseconds once
the membrane distance was smaller than ∼5 nm. A high
transmembrane voltage induced by close membrane proximity
could cause these fast-forming transient membrane pores. The
fusion pores are able to conduct ions across membrane and
in doing so, alleviate the voltage difference which leads to

FIGURE 7 | Illustration of pore formation, evolution and selection of fusion mode proposed by our MD simulation. (A) Close contact of vesicle with presynaptic membrane pulled by the fusion proteins. **(B)** Pore formation and associated release of neurotransmitters once the membrane distance, D, is smaller than a critical value. **(C)** Resealing of the fusion pores after the release of neurotransmitters for a KR fusion. **(D)** Formation of stalk-like structure for hemifusion appears when the membrane distance is further reduced. **(E)** Full fusion can be achieved by either expansion of the fusion pore (**B** under a larger lateral force), or following the hemifusion **(D)**.

final resealing of the membranes within a few nanoseconds. These sequential processes of pore formation, ion exchange, and pore healing in our MD simulations are consistent with the features of KR fusion observed in experiments (Zhang et al., 2009). In addition, we showed that the applied force on the membrane from native proteins plays a crucial role in modulating the stability and lifetime of fusion pores and may regulate the ultimate fusion mode to either KR fusion or FF. Therefore, both the pore formation and evolution for membrane fusion are tightly controlled by fusion proteins in physiological conditions.

AUTHOR CONTRIBUTIONS

DL and BJ designed research; BB, ZT, and DL performed research; BB, ZT, DL, and BJ analyzed data; BB, ZT, DL, and BJ wrote the paper. All authors reviewed the manuscript.

SUPPLEMENTARY MATERIAL

The Supplementary Material for this article can be found online at: http://journal.frontiersin.org/article/10.3389/fnmol.2016.00136/full#supplementary-material

REFERENCES

Aguilar, P. S., Engel, A., and Walter, P. (2007). The plasma membrane proteins Prm1 and Fig1 ascertain fidelity of membrane fusion during yeast mating. *Mol. Biol. Cell* 18, 547–556. doi: 10.1091/mbc.E06-09-0776

Alabi, A. A., and Tsien, R. W. (2013). Perspectives on kiss-and-run: role in exocytosis, endocytosis, and neurotransmission. *Annu. Rev. Physiol.* 75, 393–422. doi: 10.1146/annurev-physiol-020911-153305

Blumenthal, R., and Morris, S. J. (1999). The influenza haemagglutinin-induced fusion cascade: effects of target membrane permeability changes. *Mol. Membr. Biol.* 16, 43–47. doi: 10.1080/096876899294742

Bussi, G., Donadio, D., and Parrinello, M. (2007). Canonical sampling through velocity rescaling. *J. Chem. Phys.* 126, 014101. doi: 10.1063/1.2408420

Chanturiya, A., Chernomordik, L. V., and Zimmerberg, J. (1997). Flickering fusion pores comparable with initial exocytotic pores occur in protein-free phospholipid bilayers. *Proc. Natl. Acad. Sci. U.S.A.* 94, 14423–14428. doi: 10.1073/pnas.94.26.14423

Chernomordik, L. V., and Kozlov, M. M. (2003). Protein-lipid interplay in fusion and fission of biological membranes. *Annu. Rev. Biochem.* 72, 175–207. doi: 10.1146/annurev.biochem.72.121801.161504

Chernomordik, L. V., and Kozlov, M. M. (2008). Mechanics of membrane fusion. *Nat. Struct. Mol. Biol.* 15, 675–683. doi: 10.1038/nsmb.1455

Dennison, S. M., Bowen, M. E., Brunger, A. T., and Lentz, B. R. (2006). Neuronal SNAREs do not trigger fusion between synthetic membranes but do promote PEG-mediated membrane fusion. *Biophys. J.* 90, 1661–1675. doi: 10.1529/biophysj.105.069617

Devaux, P. F. (1991). Static and dynamic lipid asymmetry in cell membranes. *Biochemistry* 30, 1163–1173. doi: 10.1021/bi00219a001

Diao, J., Cipriano, D. J., Zhao, M., Zhang, Y., Shah, S., Padolina, M. S., et al. (2013). Complexin-1 enhances the on-rate of vesicle docking via simultaneous SNARE and membrane interactions. *J. Am. Chem. Soc.* 135, 15274–15277. doi: 10.1021/ja407392n

Diao, J., Grob, P., Cipriano, D. J., Kyoung, M., Zhang, Y., Shah, S., et al. (2012). Synaptic proteins promote calcium-triggered fast transition from point contact to full fusion. *eLife* 1:e00109. doi: 10.7554/eLife.00109

Diao, J., Yoon, T. Y., Su, Z., Shin, Y. K., and Ha, T. (2009). C2AB: a molecular glue for lipid vesicles with a negatively charged surface. *Langmuir* 25, 7177–7180. doi: 10.1021/la901676e

Essmann, U., Perera, L., Berkowitz, M. L., and Darden, T., (1995). A smooth particle mesh ewald method. *J. Chem. Phys.* 103, 8577–8593. doi: 10.1063/1.470117

Fesce, R., Grohovaz, F., Valtorta, F., and Meldolesi, J. (1994). Neurotransmitter release: fusion or 'kiss-and-run'? *Trends Cell Biol.* 4, 1–4. doi: 10.1016/0962-8924(94)90025-6

Frolov, V. A., Dunina-Barkovskaya, A. Y., Samsonov, A. V., and Zimmerberg, J. (2003). Membrane permeability changes at early stages of influenza hemagglutinin-mediated fusion. *Biophys. J.* 85, 1725–1733. doi: 10.1016/S0006-3495(03)74602-5

Gong, B., Choi, B.-K., Kim, J.-Y., Shetty, D., Ko, Y. H., Selvapalam, N., et al. (2015). High affinity host-guest FRET pair for single-vesicle content-mixing assay: observation of flickering fusion events. *J. Am. Chem. Soc.* 137, 8908–8911. doi: 10.1021/jacs.5b05385

Graber, Z. T., Gericke, A., and Kooijman, E. E. (2014). Phosphatidylinositol-4,5-bisphosphate ionization in the presence of cholesterol, calcium or magnesium ions. *Chem. Phys. Lipids* 182, 62–72. doi: 10.1016/j.chemphyslip.2013.11.004

Gramse, G., Dols-Perez, A., Edwards, M. A., Fumagalli, L., and Gomila, G. (2013). Nanoscale measurement of the dielectric constant of supported lipid bilayers in aqueous solutions with electrostatic force microscopy. *Biophys. J.* 104, 1257–1262. doi: 10.1016/j.bpj.2013.02.011

Gurtovenko, A. A., Anwar, J., and Vattulainen, I. (2010). Defect-mediated trafficking across cell membranes: insights from in silico modeling. *Chem. Rev.* 110, 6077–6103. doi: 10.1021/cr1000783

Gurtovenko, A. A., and Vattulainen, I. (2005). Pore formation coupled to ion transport through lipid membranes as induced by transmembrane ionic charge imbalance: atomistic molecular dynamics study. *J. Am. Chem. Soc.* 127, 17570–17571. doi: 10.1021/ja053129n

He, L., and Wu, L. G. (2007). The debate on the kiss-and-run fusion at synapses. *Trends Neurosci.* 30, 447–455. doi: 10.1016/j.tins.2007.06.012

Helm, C. A., Israelachvili, J. N., and McGuiggan, P. M. (1992). Role of hydrophobic forces in bilayer adhesion and fusion. *Biochemistry* 31, 1794–1805. doi: 10.1021/bi00121a030

Hess, B. (2008). P-LINCS: a parallel linear constraint solver for molecular simulation. *J. Chem. Theory. Comput.* 4, 116–122. doi: 10.1021/ct700200b

Humphrey, W., Dalke, A., and Schulten, K. (1996). VMD: Visual Molecular Dynamics. *J. Mol. Graph.* 14:33–38, 27–38. doi: 10.1016/0263-7855(96)00018-5

Jackson, M. B., and Chapman, E. R. (2008). The fusion pores of Ca2+ -triggered exocytosis. *Nat. Struct. Mol. Biol.* 15, 684–689. doi: 10.1038/nsmb.1449

Jahn, R., Lang, T., and Sudhof, T. C. (2003). Membrane fusion. *Cell* 112, 519–533. doi: 10.1016/S0092-8674(03)00112-0

Jo, S., Kim, T., Iyer, V. G., and Im, W. (2008). CHARMM-GUI: a web-based graphical user interface for CHARMM. *J. Comput. Chem.* 29, 1859–1865. doi: 10.1002/jcc.20945

Jo, S., Lim, J. B., Klauda, J. B., and Im, W. (2009). CHARMM-GUI Membrane Builder for mixed bilayers and its application to yeast membranes. *Biophys. J.* 97, 50–58. doi: 10.1016/j.bpj.2009.04.013

Jorgensen, W. L., Chandrasekhar, J., Madura, J. D., Impey, R. W., and Klein, M. L. (1983). Comparison of simple potential functions for simulating liquid water. *J. Chem. Phys.* 79, 926–935. doi: 10.1063/1.445869

Klauda, J. B., Venable, R. M., Freites, J. A., O'connor, J. W., Tobias, D. J., Mondragon-Ramirez, C., et al. (2010). Update of the CHARMM all-atom

additive force field for lipids: validation on six lipid types. *J. Phys. Chem. B.* 114, 7830–7843. doi: 10.1021/jp101759q

Kyoung, M., Zhang, Y., Diao, J., Chu, S., and Brunger, A. T. (2013). Studying calcium-triggered vesicle fusion in a single vesicle-vesicle content and lipid-mixing system. *Nat. Protoc.* 8, 1–16. doi: 10.1038/nprot.2012.134

Lai, Y., Diao, J., Cipriano, D. J., Zhang, Y., Pfuetzner, R. A., Padolina, M. S., et al. (2014). Complexin inhibits spontaneous release and synchronizes Ca^{2+}-triggered synaptic vesicle fusion by distinct mechanisms. *eLife* 3:e03756. doi: 10.7554/eLife.03756

Lai, Y., Diao, J., Liu, Y., Ishitsuka, Y., Su, Z., Schulten, K., et al. (2013). Fusion pore formation and expansion induced by Ca^{2+} and synaptotagmin 1. *Proc. Natl. Acad. Sci. U.S.A.* 110, 1333–1338. doi: 10.1073/pnas.1218818110

Lai, Y., Zhao, L., Bu, B., Lou, X., Li, D., Ji, B., et al. (2015). Lipid molecules influence early stages of yeast SNARE-mediated membrane fusion. *Phys. Biol.* 12:025003. doi: 10.1088/1478-3975/12/2/025003

Leontiadou, H., Mark, A. E., and Marrink, S. J. (2004). Molecular dynamics simulations of hydrophilic pores in lipid bilayers. *Biophys. J.* 86, 2156–2164. doi: 10.1016/S0006-3495(04)74275-7

Li, D., Ji, B., Hwang, K.-C., and Huang, Y. (2011). Strength of hydrogen bond network takes crucial roles in the dissociation process of inhibitors from the HIV-1 protease binding pocket. *PLoS ONE* 6:e19268 doi: 10.1371/journal.pone.0019268

Li, D., Ji, B., Hwang, K., and Huang, Y. (2010). Crucial roles of the subnanosecond local dynamics of the flap tips in the global conformational changes of HIV-1 protease. *J. Phys. Chem. B.* 114, 3060–3069. doi: 10.1021/jp1005549

Li, D., Liu, M. S., and Ji, B. (2015). Mapping the dynamics landscape of conformational transitions in enzyme: the adenylate kinase case. *Biophys. J.* 109, 647–660. doi: 10.1016/j.bpj.2015.06.059

Marx, V. (2014). A deep look at synaptic dynamics. *Nature* 515, 293–297. doi: 10.1038/515293a

McLaughlin, S., and Murray, D. (2005). Plasma membrane phosphoinositide organization by protein electrostatics. *Nature* 438, 605–611. doi: 10.1038/nature04398

Müller, M., Katsov, K., and Schick, M. (2003). A new mechanism of model membrane fusion determined from Monte Carlo simulation. *Biophys. J.* 85, 1611–1623. doi: 10.1016/S0006-3495(03)74592-5

Parrinello, M., and Rahman, A. (1981). Polymorphic transitions in single-crystals - a new molecular-dynamics method. *J. Appl. Phys.* 52, 7182–7190. doi: 10.1063/1.328693

Richards, D. A. (2009). Vesicular release mode shapes the postsynaptic response at hippocampal synapses. *J. Physiol.* 587, 5073–5080. doi: 10.1113/jphysiol.2009.175315

Risselada, H. J., and Grubmüller, H. (2012). How SNARE molecules mediate membrane fusion: decent insights from molecular simulations. *Curr. Opin. Struct. Biol.* 22, 187–196. doi: 10.1016/j.sbi.2012.01.007

Rizo, J., and Rosenmund, C. (2008). Synaptic vesicle fusion. *Nat. Struct. Mol. Biol.* 15, 665–674. doi: 10.1038/nsmb.1450

Starai, V. J., Jun, Y., and Wickner, W. (2007). Excess vacuolar SNAREs drive lysis and Rab bypass fusion. *Proc. Natl. Acad. Sci. U.S.A.* 104, 13551–13558. doi: 10.1073/pnas.0704741104

Sun, S., Wong, J. T., and Zhang, T. Y. (2011). Atomistic simulations of electroporation in water preembedded membranes. *J. Phys. Chem. B.* 115, 13355–13359. doi: 10.1021/jp206607j

Svennerholm, L. (1968). Distribution and fatty acid composition of phosphoglycerides in normal human brain. *J. Lipid Res.* 9, 570–579.

Tieleman, D. P. (2004). The molecular basis of electroporation. *BMC Biochem.* 5:10. doi: 10.1186/1471-2091-5-10

Van Der Spoel, D., Lindahl, E., Hess, B., Groenhof, G., Mark, A. E., and Berendsen, H. J. C. (2005). GROMACS: fast, flexible, and free. *J. Comput. Chem.* 26, 1701–1718. doi: 10.1002/jcc.20291

Wang, T., Smith, E. A., Chapman, E. R., and Weisshaar, J. C. (2009). Lipid mixing and content release in single-vesicle, SNARE-driven fusion assay with 1-5 ms resolution. *Biophys. J.* 96, 4122–4131. doi: 10.1016/j.bpj.2009.02.050

Weaver, J. C., and Chizmadzhev, Y. A. (1996). Theory of electroporation: a review. *Bioelectrochem. Bioenerget.* 41, 135–160. doi: 10.1016/S0302-4598(96)05062-3

Wong, J. L., Koppel, D. E., Cowan, A. E., and Wessel, G. M. (2007). Membrane hemifusion is a stable intermediate of exocytosis. *Dev. Cell* 12, 653–659. doi: 10.1016/j.devcel.2007.02.007

Xu, C., Li, D., Cheng, Y., Liu, M., Zhang, Y., and Ji, B. (2015). Pulling out a peptide chain from β-sheet crystallite: propagation of instability of H-bonds under shear force. *Acta Mech. Sin.* 31, 416–424. doi: 10.1007/s10409-015-0404-y

Yang, L., and Huang, H. W. (2002). Observation of a membrane fusion intermediate structure. *Science* 297, 1877–1879. doi: 10.1126/science.1074354

Zhang, Q., Li, Y., and Tsien, R. W. (2009). The dynamic control of kiss-and-run and vesicular reuse probed with single nanoparticles. *Science* 323, 1448–1453. doi: 10.1126/science.1167373

Zhao, W.-D., Hamid, E., Shin, W., Wen, P. J., Krystofiak, E. S., Villarreal, S. A., et al. (2016). Hemi-fused structure mediates and controls fusion and fission in live cells. *Nature* 534, 548–552. doi: 10.1038/nature18598

Zucchi, P. C., and Zick, M. (2011). Membrane fusion catalyzed by a Rab, SNAREs, and SNARE chaperones is accompanied by enhanced permeability to small molecules and by lysis. *Mol. Biol. Cell* 22, 4635–4646. doi: 10.1091/mbc.E11-08-0680